Synthesis and characterisation of three diiron tetracarbonyl complexes related to the diiron centre of [FeFe]-hydrogenase and their protonating, electrochemical investigations†

Yanwei Wang,[a] Zhimei Li,[a] Xianghua Zeng,[a] Xiufeng Wang,[a] Caixia Zhan,[a] Yinqiu Liu,[b] Xirui Zeng,[b] Qiuyan Luo[b] and Xiaoming Liu*[a]

Received (in Victoria, Australia) 24th February 2009, Accepted 28th May 2009
First published as an Advance Article on the web 10th July 2009
DOI: 10.1039/b903758f

The synthesis, characterisation of three diiron tetracarbonyl complexes, $[Fe_2(SCH_2)_2C(Me)(CH_2OR)(PNP)(CO)_4]$ (R = H and PNP = $\mathbf{L^1}$: **2**; R = H and PNP = $\mathbf{L^2}$: **3**; R = Ts and PNP = $\mathbf{L^1}$: **4**) as models for the diiron sub-unit of [FeFe]-hydrogenase are described, where OTs, $\mathbf{L^1}$ and $\mathbf{L^2}$ are toluenesulfonate, $(Ph_2P)_2NCH_2(2\text{-}C_5H_4N)$ and $(Ph_2P)_2NCH_2Ph$, respectively. These complexes are fully characterised and the structure of complex **4** is crystallographically determined. Protonation of these complexes with $HBF_4{\cdot}Et_2O$ is probed by using infrared and NMR spectroscopies which reveals that no hydride can be formed upon addition of the acid. Instead addition of excess of the acid leads to protonating the N atom of the PNP skeleton, which is a weak base due to participating conjugating interactions with the Fe–Fe centre, as revealed by crystallographic analysis. Electrochemistry of these complexes and their electrocatalytic reduction of protons are also investigated. Our results suggest that the existence of the pendant pyridine group can lower the overpotential for proton reduction but does not seem to enhance electrocatalytic efficiency in our case.

Introduction

Since the detailed structure of [FeFe]-hydrogenase was revealed a decade ago, this enzyme and its related chemistry have been under intense investigations due to the fact that this metallo-enzyme catalyses reversibly and rapidly hydrogen oxidation and evolution with high preference to the latter reaction.[1,2] In the diiron sub-unit of the H-cluster of the enzyme, the two iron atoms of low oxidation state are bridged by a non-protein three-atom dithiolate ligand and are coordinated with 3CO and $2CN^-$ ligands plus a water or OH^- occupying its vacant site in its rest state of the enzyme, Fig. 1(a).[3,4] A very recent report also suggested that this non-protein bridging linkage could be dithiomethyl ether ($^-SCH_2OCH_2S^-$).[5] To mimic the possible aza-containing nature, Fig. 1(a), Rauchfuss and co-workers published their "click" chemistry, synthesis of an aza-containing model complex.[6] Since then, complexes of this type have been intensely studied.[7–10] These synthetic analogues as well as other artificial systems enabled to replicate some key structural features of the metal centre of the enzyme,[2,11–23] which shed light on understanding mechanistically the enzymatic catalysis.

It is interesting to note that in modelling the H-cluster of the enzyme and its diiron sub-unit, the potential role of some amino acid residues within the non-coordinating sphere, which may have a similar role to play in proton transfer,[24] have attracted much less attention compared to modelling the central atom of the bridgehead of the diiron sub-unit. A few systems bearing a pendant basic group have been reported to date.[25,26] Even rarer are model complexes with such a base showing hemi-labile coordination to the Fe–Fe centre.[17] Recent reports by Wang, Sun and Talarmin and their co-workers have shown that there were dynamic interactions between internal bases and metal hydride of its host model complex.[27,28]

In modelling the diiron centre, both monodentate phosphine ligands (PMe_3, PPh_3, $P(OEt)_3$ PMe_2Ph)[29–34] or bidentate ligands (dppm, dppe, dcpm, dppb)[35–42] have widely been used as replacement of the cyanide. These phosphine-based ligands not only more or less provide the needed electron density as does CN^- in the enzyme, but also serve as scaffolds to introduce internal bases. Among the bidentate

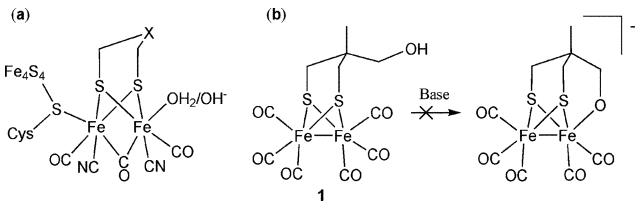

Fig. 1 (a) The H-cluster of [FeFe]-hydrogenase (X = NH, CH_2 or O) and (b) attempt to synthesise a model complex possessing Fe(I)–OR (R = organic moiety) bond for the diiron centre of the enzyme.

[a] *Department of Chemistry/Institute for Advanced Study, Nanchang University, Nanchang 330031, China. E-mail: xiaoming.liu@ncu.edu.cn; Fax: +86 (0)791 3969254; Tel: +86 (0)791 3969254*
[b] *School of Chemistry and Chemical Engineering, Jinggangshan University, Ji'an 343009, China*

† Electronic supplementary information (ESI) available: Spectral and electrochemical details. CCDC reference number 705858 (complex **4**). For ESI and crystallographic data in CIF or other electronic format see DOI: 10.1039/b903758f

phosphine ligands, PNP and PCP ligands, in which two phosphorus atoms are linked by either a sp^2 hybridised N atom or a methylene (CH_2) group, have a very small bite angle. These ligands were employed for both mono-[43,44] and diiron complexes[36,42] in the catalytic chemistry related to hydrogen activation or evolution.

Without success in an attempt of synthesising a model complex (**1**) possessing a Fe(I)–O(R) (R = organic moiety) bond, Fig. 1(b), by using a hexacarbonyl diiron complex with an alcoholyl group reported earlier, $[Fe_2\{(SCH_2)_2CMe(CH_2OH)\}(CO)_6]$, **1**,[17] we turned our attention to incorporate a PNP diphosphine ligand with a pendant pyridinyl group, $\mathbf{L^1}$, $(Ph_2P)_2NCH_2(2\text{-}C_5H_4N)$, into this complex to examine how the derived complex behaves upon protonation and how the pendant internal bases affect its electrocatalytic reduction of protons. For comparison, another diphosphine ligand, $\mathbf{L^2}$, $(Ph_2P)_2NCH_2Ph)$, was also employed. In this ligand, the pendant pyridinyl group was replaced by a phenyl group. Substitution reactions of these ligands with complex **1**, give complexes **2**, $[Fe_2\{(SCH_2)_2CMe(CH_2OH)\}\mathbf{L^1}(CO)_4]$ and **3**, $[Fe_2\{(SCH_2)_2CMe(CH_2OH)\}\mathbf{L^2}(CO)_4]$, respectively. To look into how the organic moiety of the bridgehead of the diiron hexacarbonyl complex may affect the substitution reactivity by the PNP ligand ($\mathbf{L^1}$) and hence the electrochemistry of the substituted complex, we also synthesised another diiron hexacarbonyl complex **1Ts**, $[Fe_2\{(SCH_2)_2CMe(CH_2OTs)\}(CO)_6]$ (Ts = toluenesulfonyl group). From this complex, complex **4**, $[Fe_2\{(SCH_2)_2CMe\text{-}(CH_2OTs)\}\mathbf{L^1}(CO)_4]$, was derived, which is an analogue of complexes **2** and **3**. The synthesis and characterisation of the three complexes, **2**, **3** and **4** are described and their protonating and electrochemical mechanisms probed by using infrared spectroscopic, cyclic voltammetric and digital simulating techniques. Electro-catalysis of the three complexes on proton reduction was also investigated.

Results and discussion

Synthesis of ligands L^1, L^2 and the diiron tetracarbonyl complexes 2, 3 and 4

Ligand $\mathbf{L^1}$, $(Ph_2P)_2NCH_2(2\text{-}C_5H_4N)$, was prepared at −78 °C by using methyl lithium to deprotonate pyridine-2-ylmethanamine.[45] Our practice has shown that this ligand and its phenyl analogue, $\mathbf{L^2}$, $(Ph_2P)_2N(CH_2Ph)$, could be prepared under much milder reaction conditions in high yields (Scheme 1).

Heating a solution of the diiron hexacarbonyl complexes in dry toluene with a slight excess of the ligand ($\mathbf{L^1}$ or $\mathbf{L^2}$) afforded the desired disubstituted complexes, **2**, **3** and **4** in moderate to high yields, Scheme 2. IR monitoring showed that the reaction was completed in 2 h for complexes **2** and **3**. However, the preparation of complex **4** took a much longer

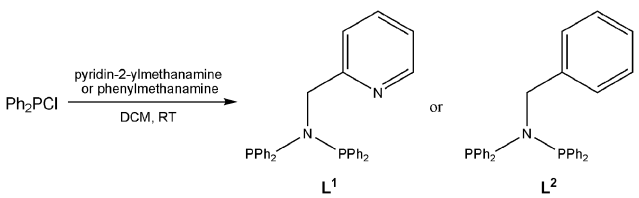

Scheme 1 Synthesis of the ligands $\mathbf{L^1}$ and $\mathbf{L^2}$.

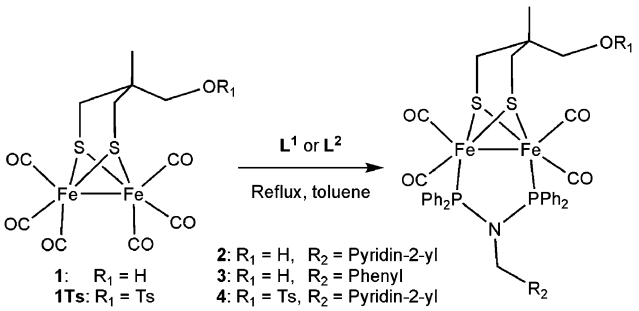

Scheme 2 Synthesis of complexes **2**, **3** and **4**.

time. The reaction sluggishness is mainly attributed to steric hindrance from the OTs group. All three complexes show four characteristic absorption bands of diiron tetracarbonyl complexes in the region between 1910 and 2000 cm^{-1}.[36–38,42] Due to the electron-withdrawing nature of both the pyridine and the OTs groups, the infrared absorption bands for complexes **2** and **4** shift towards higher frequencies by 2 and 5 cm^{-1} on average, respectively, compared to that for complex **3**. ^{31}P NMR for the three complexes showed a nearly identical single peak at about 120 ppm due to the rigidity in conformation and electronic similarity in these complexes. This is in agreement with other disubstituted diiron tetracarbonyl complexes.[38,42]

X-Ray single-crystal diffraction analysis

Among complexes **2**, **3** and **4**, complex **4** was the most readily crystallised to produce single crystals suitable for X-ray single crystal diffraction analysis. In the refinement of the crystal structure, 59 restraints were used. All hydrogen atoms except those of water, which was refined with H–O distances at 0.85 Å and with $U_{iso}(H) = 1.5U_{eq}(O)$, were positioned geometrically and treated as riding on their parent atoms with C–H distances of 0.97 Å (ethyl), 0.96 Å (methyl) and 0.93 Å (aromatic rings) and with $U_{iso}(H) = 1.2U_{eq}(C)$ (ethyl and aromatic rings) and $U_{iso}(H) = 1.5U_{eq}(C)$ (methyl). Atoms C10, C11, C6, C7, C8 and C9 of the phenyl ring of the tosyl group were refined to have approximately equal anisotropic displacement parameters. The three adjacent atoms, N2, C22 and C18 of the pyridine ring were refined in the same manner.

The crystallographic data for complex **4** are summarised in Table 1 and selected bonding parameters are tabulated in Table 2. The structural view of this complex is shown in Fig. 2. In the unit cell, some water molecules are also found, which may be accidentally introduced during crystallisation. As shown in Fig. 2, due to the bulkiness of the Ts group, it unsurprisingly points away from the Fe–Fe centre and is approximately opposite to the PNP moiety. The two phosphorus atoms coordinate to the metal at a basal–basal position and form a planar conformation together with the N1 atom due to the rigidity of the ligand conformation. Three N1-centred bond angles composed by P1, P2 and C17 are nearly perfectly equal to 120°. Furthermore, the two P–N1 bond lengths are about 1.7 Å showing that they have partial double bond character. All these bonding features suggest that the atom N1 takes an ideal sp^2 hybridisation and forms a conjugating system within the plane composed by {Fe1–Fe2–P1–N1–P2}

Table 1 Crystallographic details for complex **4**

Empirical formula	$C_{46}H_{46}Fe_2N_2O_9P_2S_3$
M	1040.70
T/K	293(2)
λ/Å	0.71073
Crystal system	Monoclinic
Space group	*Cc*
a/Å	13.5760(18)
b/Å	20.7486(18)
c/Å	17.305(3)
β/°	98.192(2)
V/Å^3	4824.8(11)
Z, D_c/Mg m^{-3}	4, 1.433
μ/mm^{-1}	0.853
F(000)	2152
Crystal size/mm	0.26 × 0.16 × 0.08
θ range for data collection	1.81–26.00
Limiting indices, *hkl*	−16 to 16, −25 to 25, −20 to 21
Reflections collected/unique	15 465/8600 (R_{int} = 0.0706)
Completeness (%) to θ = 26.00°	98.4
Absorption correction	None
Refinement method	Full-matrix least-squares on F^2
Data/restraints/parameters	8600/59/579
Goodness-of-fit on F^2	0.995
Final R indices [$I > 2\sigma(I)$]	R_1 = 0.0644, wR_2 = 0.1471
R indices (all data)	R_1 = 0.1194, wR_2 = 0.1609
Absolute structure parameter	0.05(3)
Largest diff. peak, hole/e Å^{-3}	0.749, −0.709

Table 2 Selected bond lengths (Å) and angles (°) for complex **4**

Fe(1)–P(2)	2.2029(15)	Fe(2)–S(2)	2.2493(15)
Fe(2)–P(1)	2.2025(15)	Fe(2)–S(1)	2.2548(16)
Fe(1)–S(1)	2.2605(15)	P(1)–N(1)	1.744(4)
Fe(1)–S(2)	2.2878(16)	P(2)–N(1)	1.711(4)
Fe(1)–Fe(2)	2.4807(11)		
S(1)–Fe(1)–S(2)	82.48(5)	N(1)–P(1)–Fe(2)	114.30(15)
P(1)–Fe(2)–Fe(1)	94.64(5)	N(1)–P(2)–Fe(1)	112.29(14)
P(2)–Fe(1)–Fe(2)	98.26(5)	Fe(2)–S(1)–Fe(1)	66.65(5)
S(1)–Fe(1)–Fe(2)	56.56(4)	Fe(2)–S(2)–Fe(1)	66.28(5)
S(2)–Fe(1)–Fe(2)	56.11(4)	C(17)–N(1)–P(2)	120.2(3)
S(2)–Fe(2)–S(1)	83.47(6)	C(17)–N(1)–P(1)	120.5(3)
S(2)–Fe(2)–Fe(1)	57.60(4)	P(2)–N(1)–P(1)	119.4(2)
S(1)–Fe(2)–Fe(1)	56.78(4)		

via d_π–p_π–d_π interaction, which renders this N atom weak basicity (*vide infra*). These results are in agreement with other PNP analogues.[42] As indicated in Table 2, typical bond lengths and angles related to the Fe and S atoms are generally similar to those of diiron tetracarbonyl analogues.[36–38,42] However, it is noteworthy that the Fe–Fe bond length in this PNP containing complex **4** is shorter by 0.04 Å compared to that of the PCP containing analogues,[36,38] where C represents a CH_2 group, in spite of the smaller bond angle of 115° for ∠PCP compared to *ca.* 120° for ∠PNP in complex **4**. This bond shortening is attributed to the stronger electronic interaction stemming from their conjugating interaction within the five-membered ring, which does not exist in the PCP analogues.

Protonation of complexes 2, 3 and 4

The protonation reactions of complexes **2**, **3** and **4** were performed in acetonitrile by using $HBF_4{\cdot}Et_2O$. Upon the addition of one equivalent of the acid, infrared absorption bands of complexes **2** and **4** shifted towards higher energy by

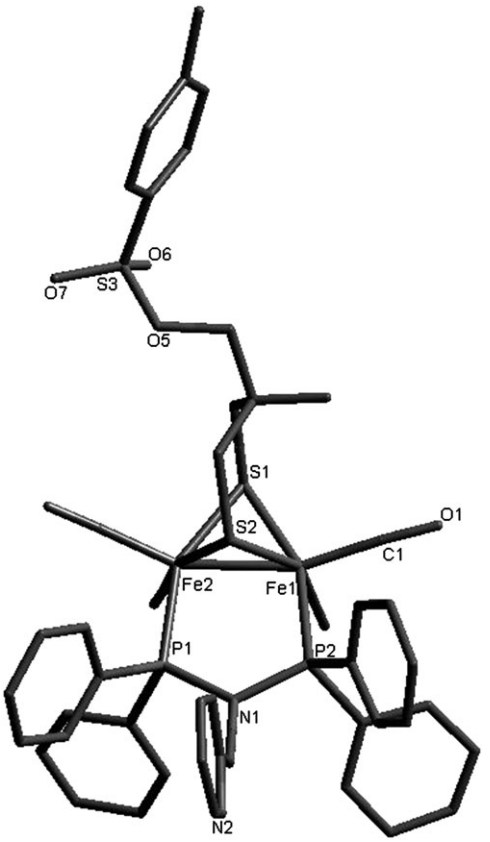

Fig. 2 Structural view of the model complex **4** (for clarity a stick model is adopted and hydrogen atoms are excluded).

about 5 cm^{-1} (Fig. S2, ESI†) whereas for complex **3**, its infrared spectrum was unchanged (Fig. 3). This shows evidently that the pyridinyl N atom in complexes **2** and **4** is more basic than the other N atoms. However, upon addition of the acid to over 15 equivalents, the infrared absorption bands of all the three complexes shifted to higher frequencies compared to parent complexes by about 40 cm^{-1}, Fig. 3 and Fig. S2 (ESI†). These protonated species are not very stable since neutralisation with triethylamine restored only partially

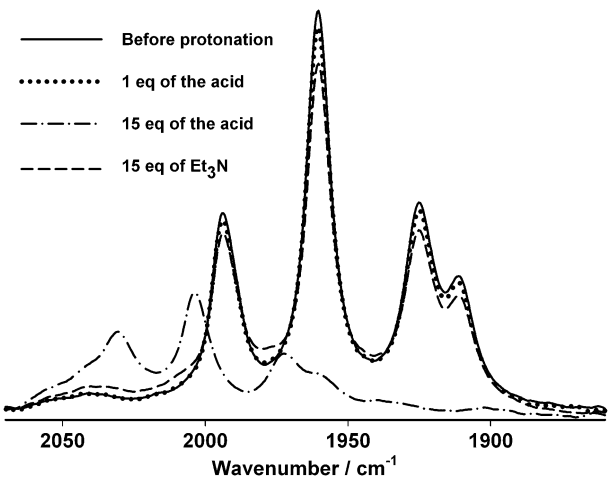

Fig. 3 Protonation of complex **3** and its restoration upon the addition of Et_3N in acetonitrile.

their parent complexes as judged by variations in infrared band intensities before protonation and after neutralisation. In one occasion, this recovery was over 80% for complex **3**, Fig. 3. It is noteworthy that these protonated species have a rather similar spectral profile to that of their parent complexes. Linear correlations are found between the absorption bands of the protonated and those of their parent complexes, Fig. S3 (ESI†). This indicates that there is no significant change in geometries upon the protonation when excess of the acid is used.[17]

The question is where the proton is located in these instable species. It has been known that direct protonation of the Fe–Fe bond to form a hydride causes a "blue" shift for carbonyl stretching frequencies by about 80 cm^{-1} for either diiron pentacarbonyl or tetracarbonyl complexes.[17,29,36,37,46] This is about 2-fold higher than the 40 cm^{-1} observed in this work. Further, the spectral profile of these species derived from the three complexes differ significantly from that of those hydrides which usually comprise two major bands centred at about 2020 cm^{-1}.[26,29,30,46] NMR spectroscopy did not show any hydride signals even at −40 °C in the upfield region where signals for iron hydrides appear usually.[17,36,37] All these experimental observations show that these unstable protonated species are not metal hydrides. One of the remaining sites for these protonated species is the N atom of the PNP skeleton. In fact, the frequency shift (40 cm^{-1}) is somewhat comparable with that (*ca.* 18 cm^{-1}) of protonated aza-containing analogues.[8,9,29,47,48] The slightly larger shift for complexes **2**, **3** and **4** is attributed to that the N atom of the PNP skeleton is closer to the metal centre by one σ-bond distance compared to those of aza-containing analogues. There was a report that the bridging thiolate in diiron complexes could be also protonated and caused a huge "blue" shift in CO stretching frequencies up to 150 cm^{-1};[49] this however did not occur for complexes **2**, **3** and **4**.

For other diiron tetracarbonyl complexes with bidentate diphosphine ligands of the skeletons $P(CH_2)_nP$ (where n = 1, 2 and 4) reported by Hogarth and co-workers, stable hydrides were hardly observed.[36,37] There was only one exception that two substituents on each phosphorus atom of the PCP ligand were cyclohexyl group, and this was attributed to the electron-rich nature of the cyclohexyl group.[36] The general difficulty for hydride formation for the diiron complexes with either PCP or PNP ligands was attributed to the following two factors: electron density on the Fe–Fe centre and the rigidity of the conformation of these ligands.[37] However, we believe that a steric effect is the major governing factor, based on following two arguments, (i) our recent report showed that diiron pentacarbonyl complexes, whose infrared absorption bands were at least 50 cm^{-1} higher than those of complexes **2**, **3** and **4**, formed reasonably stable bridging hydrides,[17] and (ii) other disubstituted analogues with two monodentate phosphine ligands also readily formed bridging hydrides.[26,29,30,46] In the sense of a steric effect, both the bulkiness of the substituents and the length of the linker between the two phosphorus atoms determine the ease of hydride formation. These observations may serve as supportive evidence of the protonating pathway proposed recently by both Talarmin and Hogarth.[27,35]

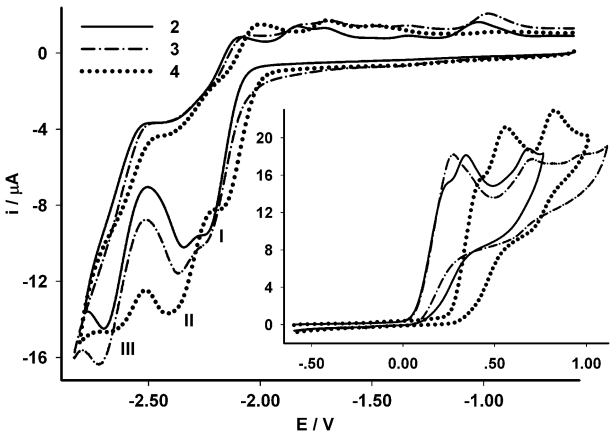

Fig. 4 Cyclic voltammograms of complexes **2**, **3** and **4** at 3.0, 4.0 and 4.0 mM, respectively in 0.5 M $[NBu_4]BF_4$/THF. Inset: the oxidation processes of the three complexes.

Electrochemistry of complexes 2, 3 and 4

The electrochemistry for complexes **2**, **3** and **4** is presented in Fig. 4. As shown in Fig. 4, complexes **2** and **3** exhibit some similarity in electrochemical profiles and show multiple reductions and oxidations. Due to the similarity of complexes **2** and **3** in coordinating ligands, their reduction processes are nearly superimposable. The presence of the tosyl group in complex **4** affects significantly the electrochemical behaviour. For the convenience of discussion, the three reduction processes of these complexes are designated as processes **I**, **II** and **III** as illustrated in Fig. 4. All related redox peak potentials are tabulated in Table 3.

Recently, Talarmin, Schollhammer and their co-workers thoroughly investigated the electrochemistry of an analogous complex and proposed that their diiron tetracarbonyl complex followed an EE mechanism coupled with disproportionation of the monoanion, and the reduction process at the most negative potential was attributed to the reduction of a daughter product associated with reductions at more positive potentials.[50] For the two successive reductions described in this mechanism, the separation of their peak potentials depends on the thermostability of the monoanion and the second reduction potential could be more positive than the first one.[51–54] Since the complexes studied in this work possess structural similarity with those reported,[50] it is sensible to assume that these complexes may follow similarly this electrochemical mechanism. To rationalise this assumption, electrochemical investigations and digital simulations were carried out.

For process **I**, there is no doubt for its assignment to the reduction of the parent complexes. For the reduction **II**, there are two possibilities, that is, one is the further reduction of the monoanion as suggested in the mechanism above,[50] and the other a daughter product generated from the decomposition of the monoanion. The observation that increasing scanning rate enhanced process **II**, Fig. 5, implies that process **II** is due to the further reduction of the monoanion. By switching the working atmosphere from Ar to CO, Fig. 6, the great suppression of process **III** shows that it was associated with chemical reaction(s) of either the monoanion

Table 3 Redox peak potentials (V) of the diiron complexes **2**, **3** and **4** under Ar and CO atmospheres, respectively

	Under Ar atmosphere			Under CO atmosphere		
	Reduction	Oxidation[a]	Oxidation	Reduction	Oxidation[a]	Oxidation
2	−2.70, −2.34, −2.25	−2.09, −1.83, −1.70, 1.33, −1.02	0.24, 0.35, 0.68	−2.66, −2.38, −2.27	−2.04, −1.11	0.26, 0.36, 0.69
3	−2.72, −2.36, −2.27	−2.05, −1.80, −1.69, −1.35, −0.98	0.27, 0.70, 0.98	−2.64, −2.31, −2.21	−2.04, −1.30, −1.16	0.23, 0.73, 1.01
4	−2.67, −2.41, −2.19	−2.00, −1.70, −1.47	0.42, 0.55, 0.83	−2.61, −2.29, −2.12	−1.98, −1.09	0.40, 0.53, 0.78

[a] Oxidation processes related to the reduction processes **II** and **III**.

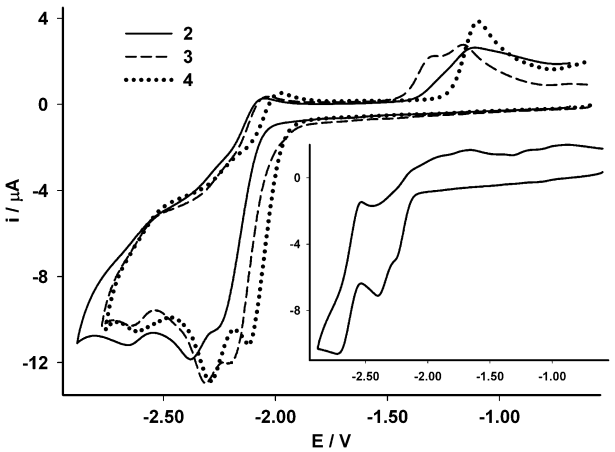

Fig. 5 Cyclic voltammograms of complexes **2**, **3** and **4** at 6.3, 6.9 and 6.8 mM, respectively under CO atmosphere. Inset: the cyclic voltammogram of complex **2** (3.8 mM) at low temperature (253 K) under Ar atmosphere.

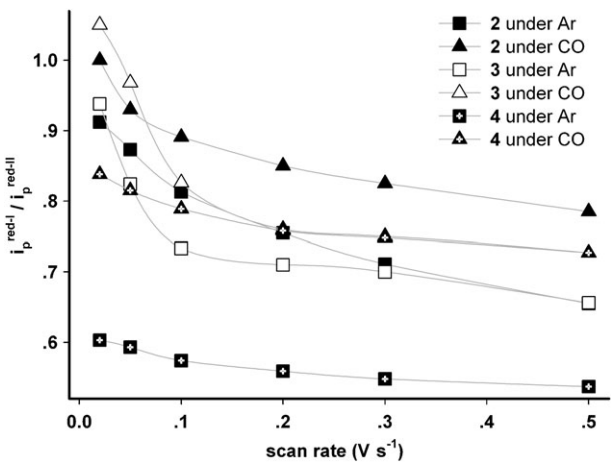

Fig. 6 Plot of the $i_p^{red\text{-}I}/i_p^{red\text{-}II}$ ratio of complexes **2**, **3** and **4** *vs.* scanning rate under Ar or CO atmosphere.

or the dianion, or perhaps both, involving CO-loss. Under the same conditions, process **II** did not show noticeable change as shown in Fig. 6 and Fig. S4 (ESI†) for complexes **2** and **3** whereas for complex **4**, process **II** was significantly suppressed, which suggests that this complex may follow a mechanism different from that for the other two complexes. Indeed, among the three complexes, complex **4** has the largest separation in peak potential between the reductions **I** and **II** and thus probably the most stable monoanion.[52] The improvement in stability of the monoanion can be ascribed to both electronic and steric causes. The former stems from the electron-withdrawing nature of the OTs group in the bridgehead which renders the diiron centre more tolerant towards reduction and the latter from the bulkiness of the OTs group which may disfavour a disproportionation reaction of the monoanion.

Although the above discussions suggest that processes **I** and **II** generally follow the disproportionation mechanism,[50] what the origin of process **III** is and how CO is involved in the related chemical processes are not clear. To shed some light on these questions, digital simulations were performed by following the disproportionation mechanism under both Ar and CO atmospheres. The simulation was started with the first reduction and thermodynamic parameters were finely tuned so that under both Ar and CO atmospheres, there was a globally satisfactory fit and minimal discrepancy between the experimental and simulated cyclic voltammograms. Then the simulation was further performed to include the second reduction, process **II**. For complex **3**, the comparison between the experimental and simulated cyclic voltammograms are shown in Fig. 7 and Fig. 8 under Ar and CO atmospheres, respectively. For complex **2**, the results are shown in Fig. S6 and Fig. S7 (ESI†). The mechanism followed in the simulations is shown in Scheme 3 and related thermodynamic parameters are tabulated in Table 4. As shown in Fig. 7 and Fig. 8, and Fig. S6 and Fig. S7 (ESI†), the proposed mechanism generally describes the chemical and electrochemistry at least for processes **I** and **II**. Simulated results at various scanning rates are shown in Fig. S4 (ESI†).

However, attempts to incorporate process **III** into the mechanism by assuming that the reduction was attributed to either decomposed product **P1** or **P2** failed to generate

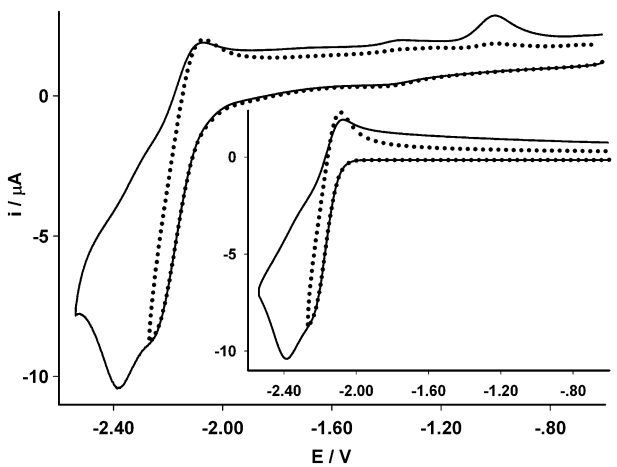

Fig. 7 Cyclic voltammograms of complex **3** at various scanning potential ranges under Ar atmosphere (inset: simulated ones).

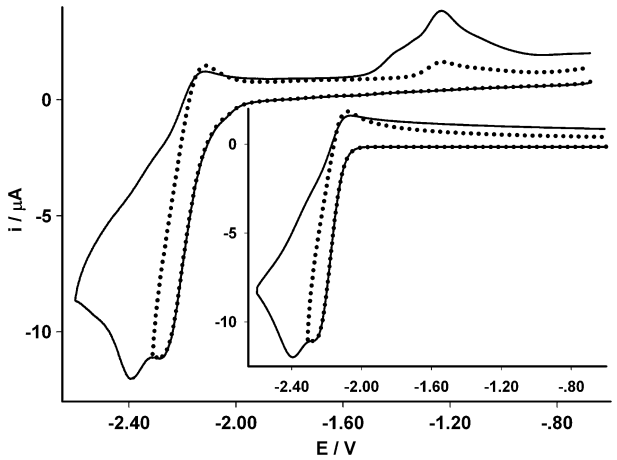

Fig. 8 Cyclic voltammograms of complex **3** at various scanning potential ranges under CO atmosphere (inset: simulated ones).

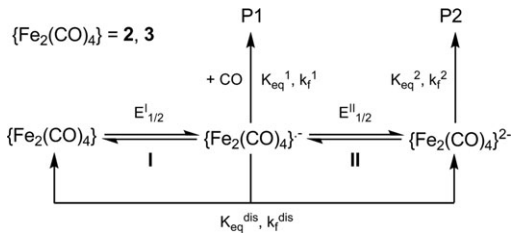

Scheme 3 Proposed electrochemical mechanism for complexes **2** and **3**; **P1** and **P2** are daughter products derived from related chemical reactions.

Table 4 Thermodynamic parameters for the electrochemistry and related chemical processes of complexes **2** and **3** generated from digital simulation

Entry	$E^{I}_{1/2}$	k_s[a]	$E^{II}_{1/2}$	k_s[a]	K_{eq}^{dis}	k_f^{dis}	K_{eq}^{1}	k_f^{1}	K_{eq}^{2}	k_f^{2}
2	−2.14	0.0075	−2.25	0.0016	0.013	800	60	20	1500	40
3	−2.16	0.0035	−2.31	0.0023	0.003	1200	300	120	1300	100

[a] Intrinsic electron transfer constant.

satisfactory results. The major problem encountered was that the generated reduction peak was far weaker than the experimentally observed peak. CO-suppression effect in the simulations also did not match the experimental observations even when CO-loss was introduced into the decomposition of the dianion. This suggests that the species which gives reduction **III** is derived from further reactions associated significantly with CO-loss, probably involving **P1** and/or **P2**. It is hard to identify the species responsible for process **III** due to the complexity. However, it is noteworthy that this species shows better reversibility at low temperature, Fig. 6 (inset). There were reports that reduction of diiron carbonyl complexes were followed by chemical reactions which might give tetrairon species.[55,56] It was also known that polynuclear iron clusters often exhibited reversible reductions.[57,58] Thus, we speculate that this species is probably a polynuclear product.

For complex **4**, as described earlier, the tosyl group has profound influence on its electrochemical behaviour. This is particularly significant under Ar atmosphere. As shown in Fig. 4, close examination of process **II** reveals that it is broader compared to the analogous peaks of the other two complexes. Although following a similar mechanism to that for complexes **2** and **3** did not afford a good reproduction under Ar atmosphere (Fig. S8, inset), the proposed mechanism of Scheme S1 (ESI†) seems to nicely describe the electrochemistry of the complex under CO atmosphere, Fig. S8. This indicates that the proposed mechanism omitted some unknown process(es) under Ar atmosphere, which probably contributed to the broadness of process **II** and were suppressed under CO atmosphere. Despite the unsatisfactory simulation under Ar atmosphere, the generated thermodynamic parameters shown in Scheme S1 (ESI†) indicate that the disproportionation of the monoanion is slower by one to two orders of magnitude compared to that for complexes **2** and **3**, which is in agreement with the earlier discussion that the monoanion of this complex is thermodynamically more stable.

In the above simulations, oxidations related to those reduced species were not included but Fig. 9 and Fig. S5 (ESI†) do show that multiple oxidation processes were mainly associated with two reductions, **II** and **III**, respectively. Oxidations of the parent complexes are not considered either in these mechanisms. These oxidation processes are shown in Fig. 4 (inset) and apparently involve multielectron transfer followed by chemical reactions as suggested by their significant increase in current intensity and complexity.

Electrocatalysis of proton reduction by complexes 2, 3 and 4

The electrochemical responses of complexes **2**, **3** and **4** upon the addition of the acid $HBF_4{\cdot}Et_2O$ are shown in Fig. 10. Since they possess the same protonable sites, it is not surprising that complexes **2** and **4** exhibit rather similar cyclic voltammetry in this acidic medium. As shown in Fig. 10 (top), a new broad reduction process appears at a potential more positive by over 300 mV compared to process **I** of their parent complexes. This newly appeared reduction shows electrocatalytic activity with a steady increase in peak current with acid addition. We attribute this process to the protonated form of the two complexes with a pendant pyridinium group. The effect of the positive charge of this pyridinium group on the diiron

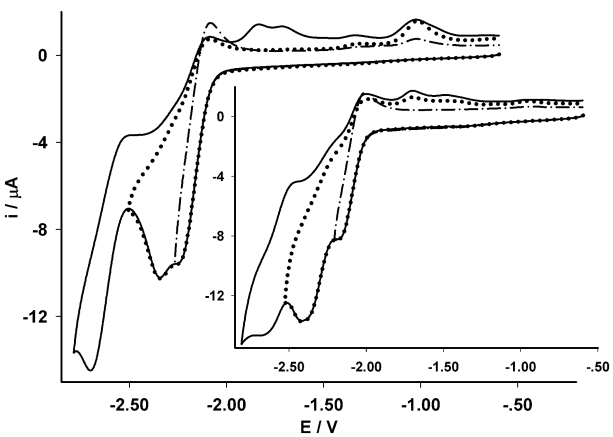

Fig. 9 Cyclic voltammograms of complexes **2** and **4** (inset) at different scanning potential ranges under Ar atmosphere, scanning rate = 0.1 V s^{-1}.

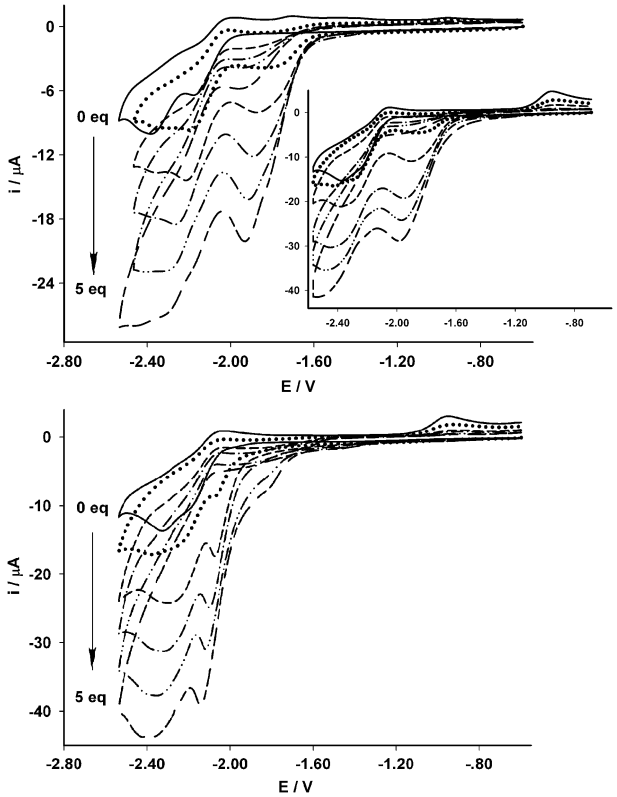

Fig. 10 Cyclic voltammograms of complexes **4** (4.3 mM) and **2** (4.0 mM) (inset) (top) and **3** (4.2 mM) (bottom) in the presence of $HBF_4{\cdot}Et_2O$ in 0.5 M $[NBu_4][BF_4]$–THF at a scan rate of 0.1 V s^{-1}.

centre drives its reduction to more positive potential.[25,26] It is clear that pre-protonation of the pendant pyridine group of the complexes is essential for this process to occur.

As suggested by the complicated electrochemistry in acidic medium, the electrochemical mechanism for complexes **2**, **3** and **4** may be more complicated than that reported recently by other researchers.[59] Best and Talarmin and their co-workers conducted detailed mechanistic studies for electrocatalysis of proton reduction catalysed by diiron hexacarbonyl complexes.[53,55] In spite of the variation in the bridgehead of the diiron complexes, the common features are that the electrocatalysis follows a multipathway to evolve hydrogen. As discussed in the electrochemistry of these complexes earlier, the diiron complexes of the moiety $\{Fe_2(CO)_{6-n}L_n\}$ (n = 0, 1 and 2; L = non-carbonyl ligand, for instance, phosphine) adopt essentially the same electrochemical mechanism as described in Scheme 3, regardless of the variations in the number of carbonyl ligands in the diiron core.[50,51,53,54] Thus, it is reasonable to assume that the complexes investigated in this work may generally follow a similar mechanism as described for those diiron hexacarbonyl complexes.[53,55] As shown in Fig. 10 (top), no substantial catalysis was observed, which implies that the protonated species $[\mathbf{HX}]^+$ is not a strong enough acid to protonate the successive reduced species. By following these considerations, multipathway mechanisms for the electrocatalysis of these complexes are presented in Scheme 4 (left panel). The multipathway nature of the mechanisms may explain the broadness of the cyclic voltammograms shown in Fig. 10.

Not surprisingly, complex **3** shows a different electrochemical response upon acid addition due to its lacking the protonable pyridine base, Fig. 10 (bottom). The distinct feature is that a sharp peak appeared at *ca.* −2.1 V, which may be attributed to process **B′** (right panel, Scheme 4) since a species generated in the catalytic reduction of protons could be reduced at a potential more positive than that of its parent diiron hexacarbonyl complex.[53,55] At higher acid concentration, a shoulder appearing prior to the main reduction may be due to absorption rather than genuine reduction related to the complex. Compared to the other two complexes, the major difference for this complex is mechanistically that the reduction of the complex is necessary prior to protonation since we did not observe formation of either any hydride or protonated species for the parent complex **3** at low acid concentration (*vide anti*).

For the possible pathways, **A**, **B** and **C** for complexes **2** and **4** (left panel), and **A′**, **B′** and **C′** for complex **3** (right panel) shown in Scheme 4, it is a non-trivial task to figure out which one is dominant and/or whether they all operate or not under the considered conditions. However, for all the complexes, the electrocatalytic current against the acid concentration shows a linear relationship with correlation coefficient >0.999, Fig. 11. As indicated by the gradients of the three plots, complexes **2** and **3** have rather similar electrocatalytic efficiency, which is about one third higher than that of complex **4**. This suggests that the pendant pyridine in both complexes **2** and **4** do not seem to improve the electrocatalytic efficiency of proton reduction except by lowering the proton reduction overpotential, Fig. 10 (top).

Conclusions

While the bulkiness of the organic moiety in the bridgehead of complexes **1** and **1Ts** significantly affects their substitution reaction with both ligands $\mathbf{L^1}$ and $\mathbf{L^2}$, protonating the Fe–Fe bond of their substituted complexes **2–4** is mainly hindered by the rigidity of the PNP ligand and the steric effect originating from the phenyl groups on the two P atoms. Of the three complexes, complexes **2** and **3** exhibit rather similar electrochemistry. The first two reduction processes may follow the mechanism recently proposed by Tarlamin and co-workers,[50] an EE process coupled with disproportionation of the monoanion to its parent complex and dianion. For complex **4**, however, reduction **II** may comprise additional unknown process(es) compared to the other two complexes, which was not further explored in this work. It is clear that process **III** for all the three complexes is associated with chemical reactions involving CO-loss. How the reactions are related to the reductions and their decomposed products is subject to further investigations.

The electrocatalytic behaviours of the three complexes have shown that the pendant pyridine group after being protonated can lower the overpotential for proton reduction but does not seem to improve the electrocatalytic efficiency for proton reduction. Recent reports by Wang, Sun, Talarmin and our own work have shown that an internal base may play a role in intramolecularly relaying protons.[17,27,28] However, as to how such a pendant base in a model complex may effectively

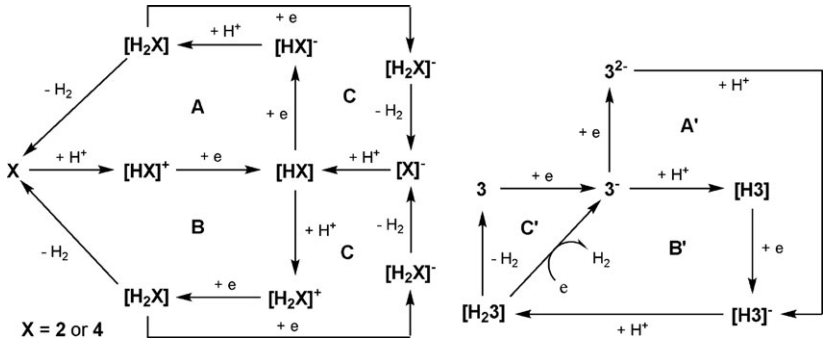

Scheme 4 Proposed electrocatalytic mechanisms for the proton reduction catalysed by the three complexes **2**, **3** and **4**.

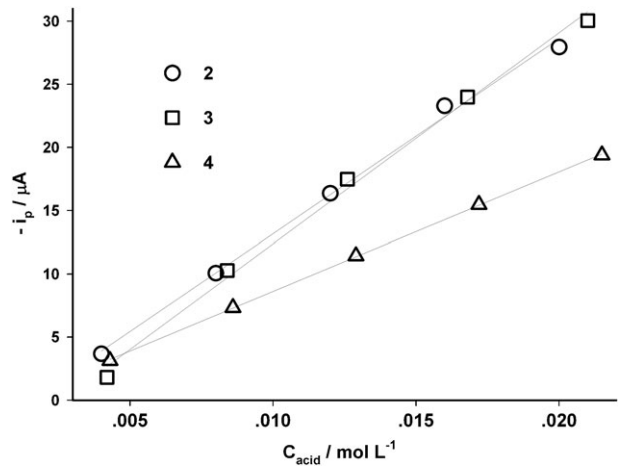

Fig. 11 Linear correlation of the electrocatalytic peak current (i_p) with the concentration of the added acid (the concentration of complexes **2**, **3** and **4** are the same as in Fig. 10).

enhance electrocatalytic efficiency of hydrogen evolution needs still further exploration.

Experimental

All reactions were carried out under Ar atmosphere with standard Schlenk techniques. Solvents were dried and distilled prior to use by following standard procedures. Triiron dodecacarbonyl and tetrafluoroboric acid/ether solution were purchased from Alfa-aesar. Other chemicals were purchased from local suppliers and further purified when necessary. Complex **1**, $[Fe_2\{(\mu\text{-}SCH_2)CMe(CH_2OH)\}(CO)_6]$ and related ligands including (4-methyl-1,2-dithiolan-4-yl)methyl-4-methylbenzenesulfonate, which was used to synthesise the complex $[Fe_2\{(\mu\text{-}SCH_2)CMe(CH_2OTs)\}(CO)_6]$ (**1Ts**), were prepared by following general methodologies.[15,17] Electrochemistry was performed under an appropriate atmosphere in 0.5 M $[NBu_4]BF_4$–THF at about 300 K unless otherwise stated. Detailed procedures were described earlier elsewhere.[60] Digital simulation was performed by using DigiElch 4.0 software. In the simulation, general criteria as described earlier were observed.[61] Infrared spectra were recorded on a Varian Scimitar 2000 spectrophotometer. ^{1}H and ^{31}P NMR ($CDCl_3$ solution) spectra were collected on a BRUKER DRX-400 NMR spectrometer, unless otherwise stated. The elemental analysis service was provided by Nanjing University (China).

Protonation reactions were performed in acetonitrile under Ar atmosphere. A typical procedure is as follows. To a solution of complex **3** (0.006 g, 0.007 mmol) in CH_3CN (2.5 mL) in a Schlenk tube was added one equivalent of $HBF_4{\cdot}Et_2O$ (1.0 μL, 0.0068 mmol) in a dropwise fashion (leading to no change in the infrared spectrum). Further addition of an excess of $HBF_4{\cdot}Et_2O$ (15 μL, 0.10 mmol) shifted the IR absorption bands from 1911, 1925, 1964, 1994 cm^{-1} to higher energy by about 43 cm^{-1}, to 1960, 1972, 2004, 2031 cm^{-1}. Neutralisation of the protonated solution by adding triethylamine (14 μL, 0.10 mmol) restored complex **3** by about 80%.

^{31}P NMR of the protonated species, produced by using excessive acid ($HBF_4{\cdot}Et_2O$), were recorded *in situ* in CD_3CN on a Bruker Advance III 600 (600 MHz) at −10 °C. For complex **2**, signals at 123.56 and 126.18 ppm were observed for the first and the second protonated species, respectively. For complex **4**, the analogous corresponding chemical shifts were at 123.37 and 125.99 ppm, respectively. For complex **3**, signals at 119.94 and 122.29 ppm were observed for the parent complex and protonated species.

In the data collection for X-ray single crystal diffraction analysis, standard procedures were used for mounting the crystals on a Bruker Apex-II area-detector diffractometer at 293(2) K. The crystals were routinely coated with paraffin oil before being mounted. Intensity data were collected using Mo-Kα radiation (λ = 0.71073 Å) at 293 K using φ- and ω-scan mode. The SAINT and SADABS programs in the APPEX 2 software package were used for integration and absorption correction.[62] The structure of complex **4** was solved by direct method using SHELXS-97 program[63] and refined on F^2 with XSHELL6.3.1, all non-hydrogen atoms being modelled anisotropically.

Synthesis of $[Fe_2\{(\mu\text{-}SCH_2)CMe(CH_2OTs)\}(CO)_6]$, 1Ts

A solution of 4-methyl-4-(toluene-4-sulfonyloxy)methyl-1,2-dithiolan (1.1 g, 3.6 mmol) and $Fe_3(CO)_{12}$ (1.8 g, 3.6 mmol) in toluene (15 mL) was allowed to stir for 12 h at 90 °C. Then the solvent was removed under reduced pressure and the crude product was purified by chromatography on silica gel with ethyl acetate–petroleum ether (1 : 3) as eluent. The complex was obtained as a red solid (0.61 g, 29%). ^{1}H NMR ($CDCl_3$): δ 0.975 (s, 3H, CH_3), 2.019 (d, J = 9.7 Hz, 1H, CCH_2S), 2.199 (d, J = 14 Hz, 2H, CCH_2S), 2.466 (s, 3H, $PhCH_3$), 3.684 (s, 2H, CCH_2O), 7.372 (d, J = 8.1 Hz, 2H, Ar*H*), 7.766

(d, J = 8.2 Hz, 2H, ArH); IR (CH_2Cl_2, ν_{CO}): 2075 (s), 2036 (s), 2003 (s), 1994 (sh) cm^{-1}.

Synthesis of $(Ph_2P)_2NCH_2(2\text{-}C_5H_4N)$, L^1 and $(Ph_2P)_2NCH_2Ph$, L^2

To a solution of chlorodiphenylphosphine (1.8 ml, 10 mmol) and triethylamine (1.4 ml, 10 mmol) in CH_2Cl_2 (30 ml) was dropwise added pyridin-2-ylmethanamine (0.54 ml, 5 mmol) at ice temperature under an atmosphere of argon. A precipitate formed immediately and the reaction mixture turned deep yellow. The reaction was further stirred for 18 h at room temperature. Removal of the solvent, triethylamine and chlorodiphenylphosphine under vacuum gave a yellow oily liquid, which was re-dissolved in CH_2Cl_2 (40 ml) and washed with degassed sodium hydroxide solution (saturated, 20 ml × 3). The organic phase was dried with anhydrous $MgSO_4$ and the solvent was removed under reduced pressure after filtration, which afforded an off-white solid. Recrystallisation of the crude product in CH_2Cl_2–MeCN at low temperature produced a white solid ($\mathbf{L^1}$, 1.78 g, 75%), which was washed with acetonitrile (10 ml × 3) and dried in vacuum. Mp 168–170 °C (uncorrected). ^{1}H NMR ($CDCl_3$): δ 4.668 (t, J = 11, 2H, CH_2), 6.647 (d, J = 7.8, 1H, ArH), 6.972 (t, J = 6.0, 1H, ArH), 7.266–7.312 (m, 13H, ArH), 7.415 (t, J = 6.7, 8H, ArH), 8.385 (d, J = 3.9, 1H, ArH). ^{31}P NMR ($CDCl_3$): δ 64.35 (s). Microanalysis for $C_{30}H_{26}N_2P_2{\cdot}0.4CH_2Cl_2$: calc. (found) (%): C, 71.53 (71.78); H, 5.29 (5.82); N, 5.49 (5.11).

The ligand $\mathbf{L^2}$ (white solid) was prepared in the same manner as described for $\mathbf{L^1}$ (yield: 2.0 g, 83%). Mp 161–163 °C (uncorrected). ^{1}H NMR ($CDCl_3$): δ 4.410 (t, J = 10 Hz, 2H, CH_2), 6.690 (s, 2H, ArH), 7.012 (s, 3H, ArH), 7.211–7.278 (m, 20H, ArH).

Synthesis of $[Fe_2(\mu\text{-}SCH_2)_2CMe(CH_2OH)(L^1)(CO)_4]$, 2

A solution of complex **1** (0.219 g, 0.5 mmol) and the ligand $\mathbf{L^1}$ (0.238 g, 0.5 mmol) in dry toluene (20 mL) was heated for 1.5 h at 110 °C under stirring. After being cooled down to room temperature, the solvent was removed under reduced pressure to give a crude product. Purification by using flash chromatography with silica gel (eluent: ethyl acetate–petroleum ether = 1 : 1) produced a red solid (0.41 g, 96%). Storing a saturated solution of the product in acetonitrile at 4 °C produced single crystals. ^{1}H NMR ($CDCl_3$): δ 1.212 (s, 3H, CH_3), 2.135 (d, J = 11.3, 1H, CCH_2S), 2.393 (d, J = 13.3 Hz, 2H, CCH_2S), 2.720 (d, J = 12.5 Hz, 1H, CCH_2S), 3.591 (s, 1H, CCH_2OH), 3.694 (s, 1H, CCH_2OH), 4.885 (t, J = 8.2 Hz, 2H, NCH_2Py), 5.617 (d, J = 7.6 Hz, 1H, ArH), 6.417–6.482 (m, 2H, ArH), 6.971 (s, 4H, ArH), 7.018 (s, 2H, ArH), 7.462 (s, 6H, ArH), 7.796 (s, 8H, ArH), 7.891 (d, J = 3.6 Hz, ArH); ^{31}P NMR ($CDCl_3$): δ 121.9 (s); IR (CH_2Cl_2) ν(CO): 1998 (s), 1964 (s), 1928 (s), 1914 (sh) cm^{-1}. Microanalysis for **2** ($C_{39}H_{36}Fe_2N_2O_5P_2S_2$): calc. (found) (%): C, 55.08 (55.00); H, 4.27 (4.23); N, 3.30 (3.24).

Synthesis of $[Fe_2(\mu\text{-}SCH_2)_2CMe(CH_2OH)(L^2)(CO)_4]$, 3

Complex **3** (a red solid, 0.34 g, 79%) was prepared in the same manner as for complex **2**. ^{1}H NMR ($CDCl_3$): δ 1.115 (s, 3H, CH_3), 2.101–2.180 (m, 2H, CCH_2S), 2.254–2.301 (m, 1H, CCH_2S), 2.485–2.510 (m, 1H, CCH_2S), 3.563 (d, J = 17 Hz, 2H, CCH_2OH), 4.475 (t, J = 8.2 Hz, 2H, NCH_2Ph), 5.925 (d, J = 7.6 Hz, 2H, ArH), 6.520 (t, J = 7.5 Hz, 2H, ArH), 6.657 (t, J = 7.1 Hz, 1H, ArH), 7.140 (d, J = 7.7 Hz, 6H, ArH), 7.458 (s, 6H, ArH), 7.720 (s, 8H, ArH); ^{31}P NMR ($CDCl_3$): δ 122.9 (s); IR (CH_2Cl_2) ν(CO): 1995s, 1962s, 1926s, 1913sh cm^{-1}. Microanalysis for **3** ($C_{40}H_{37}Fe_2NO_5P_2S_2$): calc. (found) (%): C, 56.55 (56.31); H, 4.39 (4.37); N, 1.65 (2.45).

Synthesis of $[Fe_2(SCH_2)_2CMe(CH_2OTs)(L^1)(CO)_4]$, 4

Complex **4** was synthesised as a red solid in the same manner as for complex **2** by using complex **1Ts** as precursor but the reaction was for much longer (18 h). The crude product was first purified by using flash chromatography (eluent: ethyl acetate–petroleum ether = 1 : 1) and then recrystallisation from a mixed solvent of dichloromethane and hexane (1 : 1) (0.35 g, 69%). The obtained crystals were suitable for X-ray single crystal diffraction analysis. ^{1}H NMR ($CDCl_3$): δ 1.185 (s, 3H, CCH_3), 2.051–2.387 (m, 4H, 2 × CCH_2S), 2.443 (s, 3H, PhCH_3), 3.692 (d, J = 9.3 Hz, 1H, CCH_2O), 4.615 (d, J = 9.3 Hz, 1H, CCH_2O), 4.891 (t, J = 8.3 Hz, 2H, NCH_2Py), 5.593 (d, J = 7.6 Hz, 1H, ArH), 6.444–6.495 (m, 2H, ArH), 6.963-7.027 (m, 2H, ArH), 7.360 (d, J = 7.9 Hz, 2H, ArH), 7.466 (s, 6H, ArH), 7.838 (m, 11H, ArH); ^{31}P NMR ($CDCl_3$): δ 120.0 (s); IR (CH_2Cl_2) ν(CO): 2000 (s), 1967 (s), 1931 (s), 1917 (sh) cm^{-1}. Microanalysis for **4** ($C_{46}H_{42}Fe_2N_2O_7P_2S_3$): calc. (found) (%): C, 54.99 (54.85); H, 4.21 (4.25); N, 2.80 (3.60).

Acknowledgements

We thank the Natural Science Foundation of China (Grant No. 20571038, 20871064), Centre of Analysis and Testing at Nanchang University (2005040, 2009001) and the State Key Laboratory of Coordination Chemistry at Nanjing University (China) for supporting this work.

References

1 M. Frey, *ChemBioChem*, 2002, **3**, 153–160.
2 P. M. Vignais and B. Billoud, *Chem. Rev.*, 2007, **107**, 4206–4272.
3 J. W. Peters, W. N. Lanzilotta, B. J. Lemon and L. C. Seefeldt, *Science*, 1998, **282**, 1853–1858.
4 Y. Nicolet, C. Piras, P. Legrand, C. E. Hatchikian and J. C. Fontecilla-Camps, *Struct. Fold. Des.*, 1999, **7**, 13–23.
5 A. S. Pandey, T. V. Harris, L. J. Giles, J. W. Peters and R. K. Szilagyi, *J. Am. Chem. Soc.*, 2008, **130**, 4533–4540.
6 J. D. Lawrence, H. X. Li and T. B. Rauchfuss, *Chem. Commun.*, 2001, 1482–1483.
7 H. X. Li and T. B. Rauchfuss, *J. Am. Chem. Soc.*, 2002, **124**, 726–727.
8 J. D. Lawrence, H. X. Li, T. B. Rauchfuss, M. Benard and M. M. Rohmer, *Angew. Chem., Int. Ed.*, 2001, **40**, 1768–1771.
9 S. Ott, M. Kritikos, B. Akermark, L. C. Sun and R. Lomoth, *Angew. Chem., Int. Ed.*, 2004, **43**, 1006–1009.
10 S. Jiang, J. H. Liu and L. C. Sun, *Inorg. Chem. Commun.*, 2006, **9**, 290–292.
11 E. J. Lyon, I. P. Georgakaki, J. H. Reibenspies and M. Y. Darensbourg, *Angew. Chem., Int. Ed.*, 1999, **38**, 3178–3180.
12 M. Schmidt, S. M. Contakes and T. B. Rauchfuss, *J. Am. Chem. Soc.*, 1999, **121**, 9736–9737.
13 C. Tard, X. M. Liu, S. K. Ibrahim, M. Bruschi, L. De Gioia, S. C. Davies, X. Yang, L. S. Wang, G. Sawers and C. J. Pickett, *Nature*, 2005, **433**, 610–613.

14 X. M. Liu, S. K. Ibrahim, C. Tard and C. J. Pickett, *Coord. Chem. Rev.*, 2005, **249**, 1641–1652.
15 M. Razavet, S. C. Davies, D. L. Hughes, J. E. Barclay, D. J. Evans, S. A. Fairhurst, X. Liu and C. J. Pickett, *Dalton Trans.*, 2003, 586–595.
16 D. J. Evans and C. J. Pickett, *Chem. Soc. Rev.*, 2003, **32**, 268–275.
17 F. F. Xu, C. Tard, X. F. Wang, S. K. Ibrahim, D. L. Hughes, W. Zhong, X. R. Zeng, Q. Y. Luo, X. Liu and C. J. Pickett, *Chem. Commun.*, 2008, 606–608.
18 M. Y. Darensbourg, E. J. Lyon, X. Zhao and I. P. Georgakaki, *Proc. Natl. Acad. Sci. U. S. A.*, 2003, **100**, 3683–3688.
19 F. Gloaguen, J. D. Lawrence, M. Schmidt, S. R. Wilson and T. B. Rauchfuss, *J. Am. Chem. Soc.*, 2001, **123**, 12518–12527.
20 A. Le Cloirec, S. P. Best, S. Borg, S. C. Davies, D. J. Evans, D. L. Hughes and C. J. Pickett, *Chem. Commun.*, 1999, 2285–2286.
21 T. B. Rauchfuss, *Inorg. Chem.*, 2004, **43**, 14–26.
22 I. P. Georgakaki, L. M. Thomson, E. J. Lyon, M. B. Hall and M. Y. Darensbourg, *Coord. Chem. Rev.*, 2003, **238**, 255–266.
23 J. F. Capon, F. Gloaguen, P. Schollhammer and J. Talarmin, *Coord. Chem. Rev.*, 2005, **249**, 1664–1676.
24 J. W. Peters, *Curr. Opin. Struct. Biol.*, 1999, **9**, 670–676.
25 Z. Wang, W. F. Jiang, J. H. Liu, W. I. Jiang, Y. Wang, B. Akermark and L. C. Sun, *J. Organomet. Chem.*, 2008, **693**, 2828–2834.
26 R. Mejia-Rodriguez, D. S. Chong, J. H. Reibenspies, M. P. Soriaga and M. Y. Darensbourg, *J. Am. Chem. Soc.*, 2004, **126**, 12004–12014.
27 N. Wang, M. Wang, T. T. Zhang, P. Li, J. H. Liu and L. C. Sun, *Chem. Commun.*, 2008, 5800–5802.
28 S. Ezzaher, J.-F. Capon, F. Gloaguen, F. Y. Petillon, P. Schollhammer, J. Talarmin and N. Kervarec, *Inorg. Chem.*, 2009, **48**, 2–4.
29 L. Schwartz, G. Eilers, L. Eriksson, A. Gogoll, R. Lomoth and S. Ott, *Chem. Commun.*, 2006, 520–522.
30 X. Zhao, I. P. Georgakaki, M. L. Miller, R. Mejia-Rodriguez, C. Y. Chiang and M. Y. Darensbourg, *Inorg. Chem.*, 2002, **41**, 3917–3928.
31 F. Gloaguen, J. D. Lawrence, T. B. Rauchfuss, M. Benard and M. M. Rohmer, *Inorg. Chem.*, 2002, **41**, 6573–6582.
32 S. Ott, M. Borgstrom, M. Kritikos, R. Lomoth, J. Bergquist, B. Akermark, L. Hammarstrom and L. C. Sun, *Inorg. Chem.*, 2004, **43**, 4683–4692.
33 P. Li, M. Wang, C. J. He, G. H. Li, X. Y. Liu, C. N. Chen, B. Akermark and L. C. Sun, *Eur. J. Inorg. Chem.*, 2005, 2506–2513.
34 P. Li, M. Wang, C. He, X. Liu, K. Jin and L. Sun, *Eur. J. Inorg. Chem.*, 2007, 3718–3727.
35 S. Ezzaher, J. F. Capon, F. Gloaguen, F. Y. Petillon, P. Schollhammer and J. Talarmin, *Inorg. Chem.*, 2007, **46**, 3426–3428.
36 F. I. Adam, G. Hogarth and I. Richards, *J. Organomet. Chem.*, 2007, **692**, 3957–3968.
37 F. I. Adam, G. Hogarth, S. E. Kabir and D. Richards, *C. R. Chim.*, 2008, **11**, 890–905.
38 W. M. Gao, J. Ekstrom, J. H. Liu, C. N. Chen, L. Eriksson, L. H. Weng, B. Akermark and L. H. Sun, *Inorg. Chem.*, 2007, **46**, 1981–1991.
39 W. M. Gao, J. H. Liu, B. Akermark and L. C. Sun, *Inorg. Chem.*, 2006, **45**, 9169–9171.
40 L. C. Song, Z. Y. Yang, H. Z. Bian and Q. M. Hu, *Organometallics*, 2004, **23**, 3082–3084.
41 F. I. Adam, G. Hogarth, I. Richards and B. E. Sanchez, *Dalton Trans.*, 2007, 2495–2498.
42 N. Wang, M. Wang, T. B. Liu, P. Li, T. T. Zhang, M. Y. Darensbourg and L. C. Sun, *Inorg. Chem.*, 2008, **47**, 6948–6955.
43 R. M. Henry, R. K. Shoemaker, D. L. DuBois and M. R. DuBois, *J. Am. Chem. Soc.*, 2006, **128**, 3002–3010.
44 R. M. Henry, R. K. Shoemaker, R. H. Newell, G. M. Jacobsen, D. L. DuBois and M. R. DuBois, *Organometallics*, 2005, **24**, 2481–2491.
45 D. Olbert, A. Kalisch, N. Herzer, H. Gorls, P. Mayer, L. Yu, M. Reiher and M. Westerhausen, *Z. Anorg. Allg. Chem.*, 2007, **633**, 893–902.
46 I. P. Georgakaki, M. L. Miller and M. Y. Darensbourg, *Inorg. Chem.*, 2003, **42**, 2489–2494.
47 F. J. Wang, M. Wang, X. Y. Liu, K. Jin, W. B. Dong, G. H. Li, B. Akermark and L. C. Sun, *Chem. Commun.*, 2005, 3221–3223.
48 Z. Wang, J. H. Liu, C. J. He, S. Jiang, B. Akermark and L. C. Sun, *J. Organomet. Chem.*, 2007, **692**, 5501–5507.
49 W. B. Dong, M. Wang, X. Y. Liu, K. Jin, G. H. Li, F. J. Wang and L. C. Sun, *Chem. Commun.*, 2006, 305–307.
50 S. Ezzaher, J. F. Capon, F. Gloaguen, F. Y. Petillon, P. Schollhammer and J. Talarmin, *Inorg. Chem.*, 2007, **46**, 9863–9872.
51 J. F. Capon, S. Ezzaher, F. Gloaguen, F. Y. Petillon, P. Schollhammer, J. Talarmin, T. J. Davin, J. E. McGrady and K. W. Muir, *New J. Chem.*, 2007, **31**, 2052–2064.
52 A. J. Bard and L. R. Faulkner, in *Electrochemical Methods: Fundamentals and Applications*, John Wiley & Sons Inc., New York, 2nd edn, 2001, pp. 475.
53 J. F. Capon, S. Ezzaher, F. Gloaguen, F. Y. Petillon, P. Schollhammer and J. Talarmin, *Chem.–Eur. J.*, 2008, **14**, 1954–1964.
54 M. H. Cheah, S. J. Borg and S. P. Best, *Inorg. Chem.*, 2007, **46**, 1741–1750.
55 S. J. Borg, T. Behrsing, S. P. Best, M. Razavet, X. Liu and C. J. Pickett, *J. Am. Chem. Soc.*, 2004, **126**, 16988–16999.
56 S. P. Best, S. J. Borg, J. M. White, M. Razavet and C. J. Pickett, *Chem. Commun.*, 2007, 4348–4350.
57 C. Tard, X. Liu, D. L. Hughes and C. J. Pickett, *Chem. Commun.*, 2005, 133–135.
58 T. M. Bockman and J. K. Kochi, *J. Am. Chem. Soc.*, 1987, **109**, 7725–7735.
59 L. C. Song, C. G. Li, J. H. Ge, Z. Y. Yang, H. T. Wang, J. Zhang and Q. M. Hu, *J. Inorg. Biochem.*, 2008, **102**, 1973–1979.
60 X. Wang, Z. Li, F. Peng, X. Ru, X. Zeng, Q. Luo and X. Liu, *Inorg. Chim. Acta*, 2009, **362**, 2065–2067.
61 Z. Li, X. Zeng, Z. Niu and X. Liu, *Electrochim. Acta*, 2009, **54**, 3638–3644.
62 *APEX2*, Bruker AX Inc., Madison, WI, USA, 2004.
63 G. M. Sheldrick, *SHELXS-97, Program for the solution of crystal structures*, University of Göttingen, Germany, 1997.